Terahertz Quantum Cascade Lasers as Enabling Quantum Technology

Miriam Serena Vitiello and Paolo De Natale*

Quantum cascade lasers (QCLs) represent the most fascinating achievement of quantum engineering, showing how artificial materials can be generated through quantum design, with tailor-made properties. Their inherent quantum nature deeply affects their core physical parameters. QCLs indeed display intrinsic linewidths approaching the quantum limit, and show spontaneous phase-locking of their emitted modes via intracavity four-wave-mixing, meaning that they can naturally operate as miniaturized metrological frequency rulers, also in frontier frequency domains, as the far-infrared, yet unexplored in quantum science. Here, the authors discuss the fundamental quantum properties of QCLs operating at terahertz frequencies and their key technological performances, highlighting future perspectives of this frontier research field in disruptive areas of quantum technologies such as quantum sensing, quantum metrology, quantum imaging, and photonic-based quantum computation.

1. Introduction

Quantum technology (QT) platforms, capable of exploiting non-classical states of light[1,2] or atoms[3] have been recently conceived for targeting applications in a variety of strategic fields such as simulation and computation,[4,5] communication,[6] sensing,[7] and metrology.[3,8] Miniaturized, compact and integrated QT geometries have been successfully implemented in the visible and in the near-infrared parts of the electromagnetic spectrum.[9] However, QT migration to the terahertz (THz) frequency domain is facing more fundamental obstacles, since the generation, manipulation, and detection of tiny packets of light is generally technically challenging when the involved photon energies are extremely small (<10 meV).

M. S. Vitiello
NEST, CNR – Istituto Nanoscienze and Scuola Normale Superiore
Piazza San Silvestro 12, Pisa 56127, Italy
E-mail: miriam.vitiello@sns.it

P. De Natale
CNR – Istituto Nazionale di Ottica and LENS (European Laboratory for Non-linear Spectroscopy)
Via Carrara 1, Sesto Fiorentino (FI) 50019, Italy

The ORCID identification number(s) for the author(s) of this article can be found under https://doi.org/10.1002/qute.202100082

DOI: 10.1002/qute.202100082

Despite these inherent limitations, the peculiar features of THz-frequency radiation, e.g. transmissivity through otherwise opaque materials or its non-ionizing nature, can potentially allow a number of frontier applications in quantum technologies, such as quantum-secured fast digital data transfer in opaque or harsh environments (in the presence of dust, smog, particulate) or quantum-enhanced sensitivity in spectroscopic and metrological THz setups. Consequently, the development of an integrated quantum platform comprising miniaturized THz sources and detectors can represent a paradigmatic change in quantum science.

Quantum cascade lasers (QCLs)[10] represent the most remarkable achievement of quantum engineering and allow direct generation of radiation at THz frequencies[11,12] from an electrically biased semiconductor heterostructure (**Figure 1**a). QCLs display a wide optical bandwidth (OB) (up to an octave),[13] optical power levels up to hundreds mW in CW and W -level in pulsed mode[14–16] and an intrinsically high spectral purity (intrinsic linewidths of ≈100 Hz)[17–19] (Figure 1b). THz pulses have been obtained by active mode-locking, and passive generation of optical frequency combs (FCs) has been demonstrated by intracavity four-wave-mixing (Figure 1c) in both homogeneous[18,19,20] or heterogeneous designs,[13,21,22] the latter relying on multi-tasked active regions that display similar threshold currents.[20]

Alternatively, QCLs can emit THz frequency light via intracavity difference-frequency generation in mid-infrared QCLs (THz DFG-QCLs) (Figure 1d).[23] The sources are monolithic and operate at RT, similar to other mid-IR QCLs, as a result of the $\chi^{(2)}$ nonlinearity provided by the intersubband transitions within the QCL; additionally, THz DFG-QCLs are widely tunable even once tuning the mid-IR modes on a relatively narrow range.[24,25] Depending on the mid-IR pump/signal wavelength spacing, light emission can be achieved in the whole 1–6 THz range and beyond.[26] The spectral coverage is partially influenced by the losses of the active region materials or by possible reductions in the efficiency of the THz DFG process.[27]

After their demonstration as key devices in many molecular sensing applications, QCLs recently emerged as ideal laser sources for a plethora of sophisticated applications, such as high-resolution and high-precision spectroscopy,[28] frequency metrology,[29] and, more recently, for applications in quantum science or as models for atomic quantum simulations.[30]

Most of these applications require high-frequency stability with a tight control of the frequency or phase jitter or,

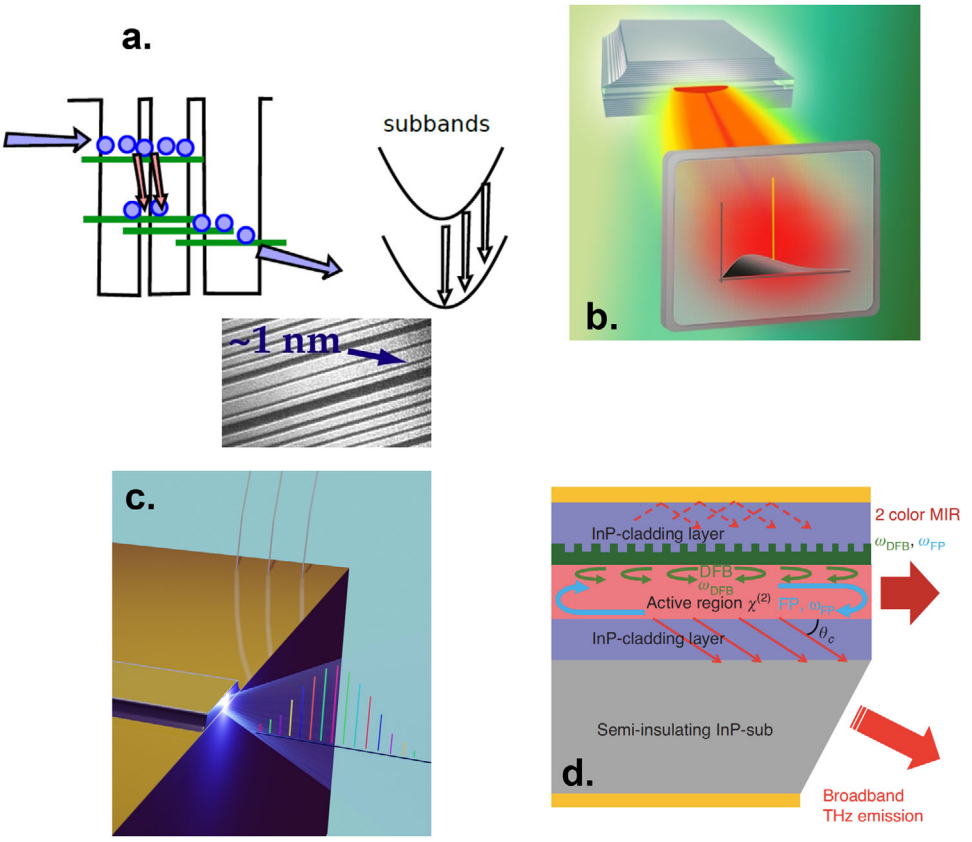

Figure 1. a) Schematic diagram of quantum cascade laser active region and energy dispersion diagram of the laser levels. The transmission electron image of a few layers is shown on the graph. b) Schematics of the intrinsically small laser linewidth of a Fabry Perot THz QCL. c) Frequency comb emission from a THz QCL. d) Schematics of a difference frequency generation THz QCL. Adapted with permission.[27] Copyright 2018, De Gruyter.

alternatively, a multi-frequency state of emission composed by a series of evenly spaced optical modes that in the frequency domain appears locked in phase.

In this review article, we will investigate the key quantum properties of THz QCL emitters, unveiling their potential role as a key technological components for future migration of QTs to the THz frequency domain.

2. Spectral Purity: Frequency Noise and Intrinsic Laser Linewidth

QCL sources have an inherent quantum nature that can be unveiled investigating a set of relevant physical parameters. As a topical example, the intrinsic linewidth of laser emission can reflect important quantum properties of such a class of lasers.

The intrinsic linewidth (LW) is, by definition, a measure of the quantum-limited fluctuations ruled by the uncertainty principle. It is also called Schawlow-Townes (S-T) linewidth and, in bipolar intra-band semiconductor lasers, it is typically affected by the variations of the refractive index of the semiconductor material due to carrier density fluctuations, which contribute to induce a significant linewidth broadening. This effect is usually accounted for by the so-called Henry or linewidth enhancement factor (α_e), that adds to the S-T linewidth inducing excess line-broadening.[31,32] Conversely, the intersubband nature of the QCLs leads to a linewidth enhancement factor which is usually very low.[33]

A clean and complete way to assess the inherent spectral purity of a single-mode QCL is the measurement of its frequency-noise power spectral density (FNPSD),[17] that allows to assess for each frequency the amount of noise contributing to the spectral width of the laser emission.[34] By performing direct intensity measurements, this technique allows to retrieve information in the frequency domain by converting the laser frequency fluctuations into measurable intensity (amplitude) variations. A discriminator is therefore needed for this purpose. It could be, for example, either a THz radiation resonant cavity,[35] or the side of a Doppler-broadened molecular transition (**Figure 2**a) while the QCL frequency is stabilized at the center of the discriminator slope.[36,17] This technique, in combination with fast detection and low-noise fast-Fourier-transform acquisition, can allow to perform spectral measurements over seven frequency decades (from 10 Hz to 100 MHz) and with 10-amplitude decades.[17]

A prototypical frequency noise power spectral density measurement, performed in a bound-to-continuum THz QCL, is shown in Figure 2b, which compares the FNPSD spectrum and the current-noise power spectral density (CNPSD) of the current driver, here converted to the same units by means of the tuning coefficient of the laser driving current.

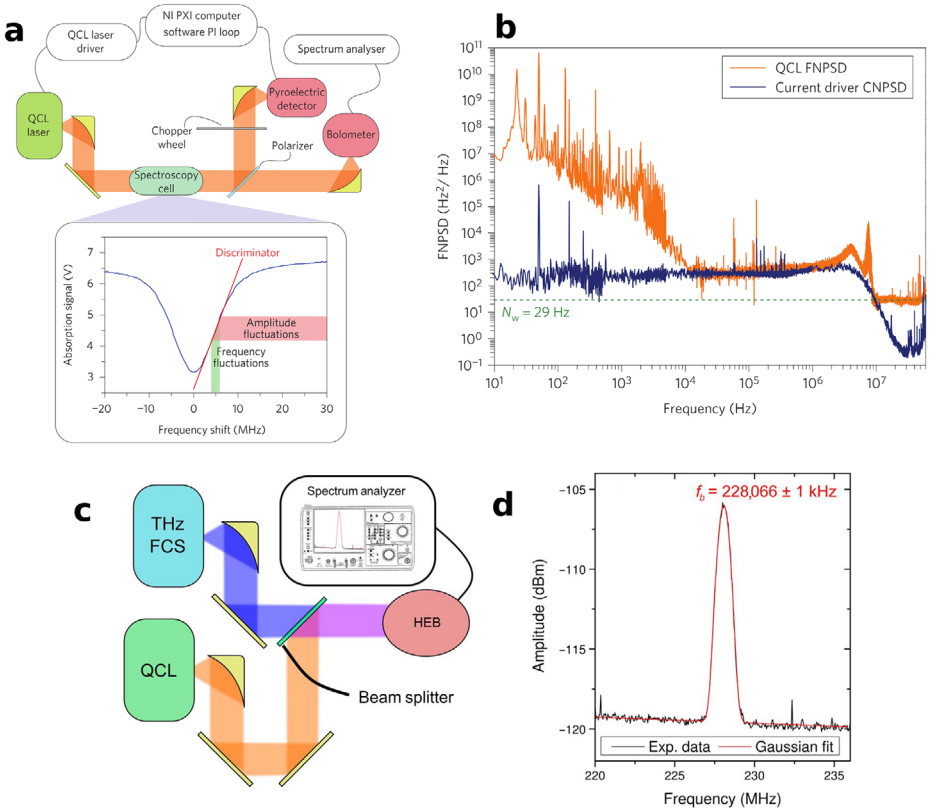

Figure 2. a) Schematic diagram of the experimental setup employed for extracting the intrinsic laser LW. The THz QCL beam is first collimated, then sent to a gas cell and finally split by a wire grid polarizer: the reflected beam, employed for frequency stabilization is first chopped and then sent to a pyroelectric detector that collects the line profile; the transmitted beam is employed for frequency-noise experiments. The bottom panel shows the discriminator function of the absorption molecular line. b) FNPSD of the THz QCL (orange trace), plotted together with the CNPSD of the current driver (blue trace, starts below the QCL FNPSD trace at lower frequencies). The dashed line marks the white noise level. (a,b) Adapted with permission.[17] Copyright 2012, Springer Nature. c) Experimental setup employed for retrieving the LW using a free space optical frequency comb synthesizer, generated in a MgO-doped lithium niobate waveguide, by optical rectification, with Cherenkov phase-matching of a femtosecond mode-locked fiber laser, working at 1.5 μm wavelength. The optical rectification process produces a zero-offset free-space THz comb with the repetition rate of 250 MHz of the pump femtosecond laser. The THz frequency comb and the emission from the DFG-QCL are overlapped on a hot electron bolometer having a 250 MHz electrical bandwidth. d) Typical beat note spectrum collected on a spectrum analyzer at 2 ms integration time. (c,d) Adapted with permission.[43] Copyright 2017, American Association for the Advancement of Science.

The FNPSD shows three distinct domains: i) in the f = 10 Hz to 10 kHz range, it is dominated by a noise that cannot be ascribed to the current driver and therefore originates from the QCL itself.[37,38] In QCLs electric field fluctuations can easily lead to a non-negligible frequency noise contribution through the gain Stark shift[39] and the cavity mode pulling effect,[40] which are often the dominant mechanisms, as confirmed by a similar dependence observed for amplitude noise. In addition, spurious contributions of low-frequency background radiation signals and/or electronic noise can also play a role; ii) in the 10 kHz–5 MHz range, the FNPSD is fully dominated by the current driver noise, since the two traces perfectly overlap; iii) above 8 MHz, the FNPSD significantly deviates from CNPSD and flattens asymptotically to a white noise level (N_w). The laser power spectrum corresponding to the white component N_w of the frequency noise is, according to the frequency noise theory, purely Lorentzian, with a FWHM $\delta\upsilon = \pi N_w$. The latter allows retrieving an intrinsic LW, $\delta\upsilon = 90 \pm 30$ Hz.[17]

Noteworthy, this technique allows forecasting the LW reduction achievable using a frequency-locking loop, assuming that its gain/bandwidth characteristics are known, while enabling to single out spurious noise sources. In fact, critical parameters affecting the QCL linewidth are all the "environmental" effects such as temperature, bias-current fluctuations, or mechanical oscillations, contributing to the so-called excess noise. This means that any experimental LW measurement, typically, is mainly dominated by extrinsic noise. Excess noise can be minimized by using frequency-stabilization or phase locking techniques, resulting in reduced laser LWs, mostly limited by the loop gain/bandwidth or by the reference width of the specific experimental system.[41]

As an alternative approach to retrieve the QCL LW on short-timescales, heterodyne mixing of the QCL with a high spectral purity, more stable laser,[42] can be used. In this latter case, the spectrum of the laser optical field can be retrieved after its down-conversion to a radio-frequency.

The latter approach was recently exploited to determine the LW of a THz QCL based on intra-cavity difference frequency generation (THz DFG-QCL).[43]

The experimental setup schematic is shown in Figure 2c, and uses one mode of an optically rectified THz frequency comb (OR-FC) as spectrally pure local oscillator for down-conversion.[42] The OR-FC is generated in a MgO-doped lithium niobate waveguide by optical rectification in the Cherenkov configuration using a femtosecond mode-locked fiber laser emitting around 1.55 μm. The optical rectification process produces a zero-offset free-space THz comb, whose spectral content is broader than the tunability range of the employed THz QCL.[44]

A fast hot-electron bolometer (HEB) is used for the heterodyne mixing (see Figure 2d for a typically retrieved signal). The experimental beat-note spectrum is then fitted by with Gaussian function that typically describes each line-shape. Since the LW of the THz comb mode involved in the beating process (≈130 Hz @ 1s, as experimentally demonstrated)[44] is negligible with respect to the emission LW of the DFG-QCL THz, the full width at half maximum (FWHM) of the Gaussian profiles gives an accurate quantitative estimation of the intrinsic emission LW, providing an upper limit of 125 kHz over a timescale of 20 μs.

This procedure inherently implies that direct information on the laser linewidth can be retrieved for specific timescales. Conversely, the use of a molecular-lineshape discriminator, combined with a FNPSD measurement, is more general and contains all relevant information on the spectral distribution of the laser frequency fluctuations. Consequently, while the laser power spectrum can be always retrieved from its frequency-noise power spectral density,[34] the opposite cannot be done.

3. Frequency Stabilization and Phase Locking of THz QCLs: Toward New Sources for Quantum Sensing

Although THz QCLs have an inherently high spectral purity,[17,45] which qualifies them as an ideal metrological source, under free running operation they typically show full width at half maximum LWs in the tens of kHz range for short timescales (few milliseconds),[46,47] while for longer integration times the LW can reach several MHz, even with stabilized temperature and under operation with low noise current drivers.

To fully exploit the potential of THz QCLs for quantum applications, it is necessary to precisely control their frequency and linewidth. Frequency-referenced, narrow-linewidth, high-power, THz frequency sources are required for high-resolution and high-sensitivity spectroscopy of molecules,[37] space science,[48] for high-precision molecular recognition and protein folding analysis[49] in biophysics, and in quantum optics and quantum computing where they could represent a key tool for controlling and manipulating cold molecular ensembles.[50]

The first report on a frequency stabilized THz QCL dates back to 2005, and made use of a molecular gas laser transition as local oscillator.[51] Since then, many different techniques and setups have been developed. Frequency-locking of a THz QCL to a molecular reference, exploiting direct-absorption spectroscopy, has been demonstrated in 2010, achieving a linewidth of 300 kHz (FWHM).[52] Soon after, linewidths of 18 kHz[53] and 240 kHz[54] have been demonstrated for a 3.5 and a 3.1 THz QCL, respectively. In all these experimental setups, the transition used as reference for locking belonged to low pressure methanol gas, usually chosen for the large number of absorption lines around the QCL emission frequency. With respect to other stabilization approaches, frequency locking to a molecular absorption has got some advantages, such as the simplicity of the implementation (as it only requires a small absorption cell and an additional fast detector) and the applicability to the whole THz domain, due to the rich absorption spectra of molecules. However, such a locking technique has provided spectral linewidths not better than tens of kHz, far away from the QCL intrinsic one (100 Hz).[17]

An alternative approach for frequency stabilizing a THz QCL relies in stabilizing a "slave" QCL source via a phase-lock loop (PLL) against a reference "master" oscillator, whose metrological properties are transferred to the locked laser. A PLL is a negative-feedback control system where the phase and frequency of the slave oscillator are forced to track those of the master one.[55] In the case of THz QCLs slave lasers, the PLL loop is usually closed on the QCL driving current, for optimal fast performances.

Among the most important master oscillators (MO) employed in combination with THz QCLs we can include molecular far-Infrared lasers,[51] frequency standards from microwave sources,[56,57] frequency standards from optical or near-infrared sources, as frequency combs. Microwave references provided a very narrow and absolute-frequency reference, suitable for mixing with THz QCLs onto sensitive cryogenic detectors, like hot-electron bolometers even with a few pW of MO radiation power.

Quantum sensing applications also require phase locking the laser emission.

Numerous approaches have been proposed to migrate FCSs to the terahertz region. As an example, detection techniques based on photo-conductive antennas[58] or electro-optic crystals[59] can allow creating a link between a continuous-wave (CW) THz source and a near-infrared comb. The beat note can be detected and phase-locked, via the CW THz source in a low-efficiency up-conversion process, with a 1 mW optical power delivered by the CW-source.

Power limitations can be overcome by producing a free-space propagating optical frequency comb[60] by directly beating it with the CW QCL source on a detector to phase-lock its emission.[44] By using a hot electron bolometer photodetector/mixer, the beat-note signal between the THz QCL and one mode of the free-standing optically rectified FC, can be retrieved in an efficient process, using only an extremely small fraction of the overall power emitted by the QCL, in the order of 100 nW.

The phase of the QCL emission is stabilized onto the frequency comb reference, via a phase-lock loop (PLL) (**Figure 3**a).[44] In this scheme, the electronic bandwidth of the loop is about 200 kHz, and the signal-to-noise ratio is >50 dB at 1Hz resolution bandwidth, close to the expected limit of 60 dB. Integrating numerically the beat-note spectra, we retrieve that ≈75% of the QCL power is phase-locked to the FCS emission. The phase-lock leads to a narrowing of most of the CW laser emission down to the THz free running comb tooth linewidth, which is only a few hertz wide (in 1 s).[61]

The achieved performance (Figure 3b) allows a 4×10^{-11} relative accuracy in the determination of the QCL frequency that can be exploited for high precision molecular spectroscopy

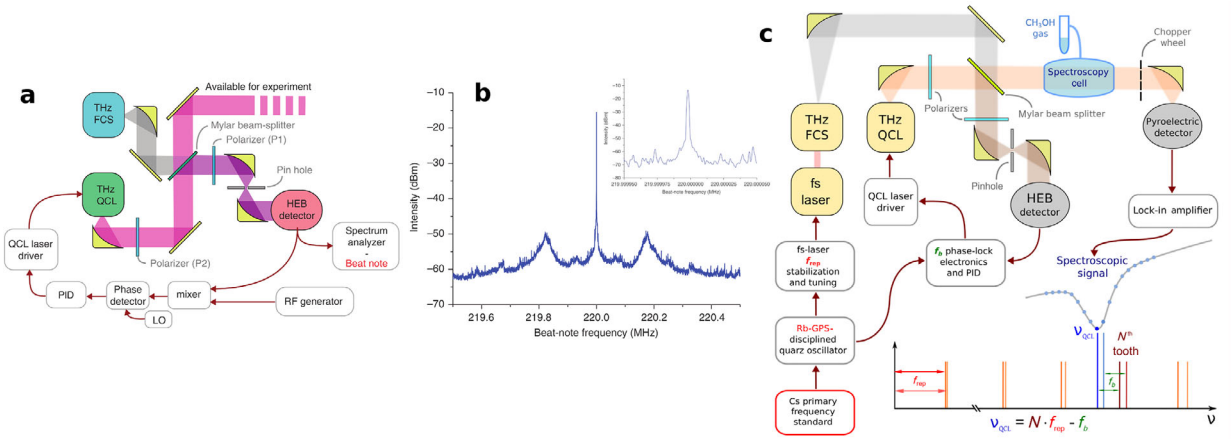

Figure 3. Phase locking. a) Experimental setup used in [28] to lock a THz QCL to one mode of a free-standing THz frequency comb. b) Width of the locked beat-note signal at 1 MHz span and 100 Hz RBW. The two sidebands identify a phase-lock electronic bandwidth of about 200 kHz. (inset) Phase-locked beat-note signal acquired with a 100 Hz span and 1 Hz RBW. (a,b) Adapted with permission.[44] Copyright 2012, Springer Nature. c) Molecular sensing experiment: the diagram describes how the traceability of the primary Cs frequency standard is transferred to the THz QCL-based spectroscopy via stabilization of the repetition rate (f_{rep}) of the pump laser and the THz frequency comb. The beat-note frequency (f_b) is kept constant by the phase lock loop, while the tuning of f_{rep} induces a proportional shift of the THz comb tooth, and thus of the QCL absolute frequency. The lock-in acquisition of the absorption signal requires the beam intensity to be mechanically modulated by a chopper. HEB, hot-electron bolometer; PID, proportional-integral-derivative controller. Adapted with permission.[28] Copyright 2014, American Physical Society.

applications[28] (Figure 3c), envisaging applications to quantum sensing and metrology. Recently, a direct-absorption spectroscopy experiment has been implemented employing methanol gas and more than 99% of the QCL emitted power. The experimental set up comprises a room-temperature pyroelectric detector, together with an optical chopper on the beam and a lock-in acquisition technique. The remaining residual fraction of the QCL power (1%) is used for the phase lock to the THz comb, following the same scheme shown in Figure 3a.

The THz comb is generated by means of a mode-locked Ti:sapphire laser, actively stabilized against a 10-MHz quartz-oscillator disciplined by a Rb-GPS clock (stability of 6×10^{-13} in 1 s and absolute accuracy of 2×10^{-12}), to transfer the stability and traceability of the Cs primary frequency standard to the Ti:sapphire repetition rate.[28] The experimentally retrieved absolute frequency scale provides an uncertainty of a few parts in 10^{-11} on the laser frequency and 10^{-9} on the line-center determination, ranking this technique as the most precise developed in the far-infrared.[28]

4. Toward New Tools for Quantum Metrology: THz Quantum Cascade Laser Frequency Combs

Broadband QCLs,[62] with heterogeneous[13,21,22] or homogeneous[18–20] active region designs, have been recently demonstrated to operate as stable miniaturized optical frequency comb synthesizers (FCs) at THz frequencies, meaning that they are spectrally characterized by a set of equidistant spectral lines, with a well-defined and stable phase relationship among each other, a carrier offset and a distinctive spectral frequency spacing.[63,64] The resulting frequency ruler can be exploited to provide a precise, direct link between optical and microwave/radio frequencies.

Such a peculiar behavior results from the large third-order $\chi^{(3)}$ Kerr nonlinearity of the QCL gain medium which, in turn, determines a robust interaction between adjacent modes via the four wave mixing (FWM) process, leading to comb formation.[65–67] However, in a free-running THz QCL, the modes are not uniformly spaced, due to chromatic dispersion.[18,68] This is a consequence of the frequency-dependent refractive index, that reflects in an index-dependent laser free spectral range.

Degenerate and non-degenerate FWM processes (**Figure 4**) induce a proliferation of modes over the whole QCL emission spectrum. The cavity modes are then injection-locked by the modes generated by FWM, ensuring correlation among all the longitudinal modes, and giving rise to a FC with a fixed phase relation, but not to a well defined pulsed emission.

At THz frequencies, the use of a broadband gain medium cannot be necessarily sufficient to overcome the dispersion of the core material itself and permit comb formation (at 3.5 THz, the group velocity dispersion (GVD) is 87,400 fs^2 mm^{-1}, that is, 250 times greater than the GVD at 7 μm (320 fs^2 mm^{-1}). In the very first demonstration[18] of a THz QCL comb, the authors integrated dispersion compensation into the QCL waveguides to cancel cavity dispersion.[18] The chirped corrugation is designed with a period chirped from short to long, that is then etched into the QCL facet (**Figure 5**a). The rationale is that long-wavelength waves, that have higher group velocities, travel to the end of the cavity before reflecting, while short-wavelength waves reflect earlier, thus compensating dispersion. The corrugation therefore mimics a double-chirped mirror that is typically used to create octave-spanning spectra in the near-infrared and visible range. The temporal evolution of the intensity, measured in the different regimes of comb operation (Figure 5b), show a different behavior in the time-domain (Figure 5c), with region I exhibiting a complex multi-pulse emission, with the blue lobe emitting only when the red lobe turns off, signature of temporal hole burning (Figure 5c). In region III, the opposite occurs: the blue lobe dominates the emission and the red lobe lases only when the blue one is off (Figure 5c). In region II, the two

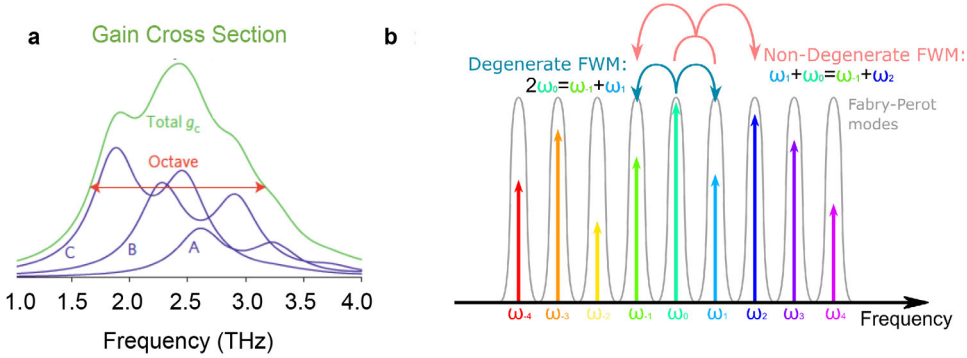

Figure 4. a) Calculated gain cross-section of a heterogeneous THz QCL. Blue curves: individual active region design labeled as A, B, C. Green curve: total active region. Adapted with permission.[13] Copyright 2014, Springer Nature. b) Schematic representation of degenerate and non-degenerate four wave mixing (FWM) responsible of the frequency comb formation mechanism. Adapted with permission.[67] Copyright 2021, De Gruyter.

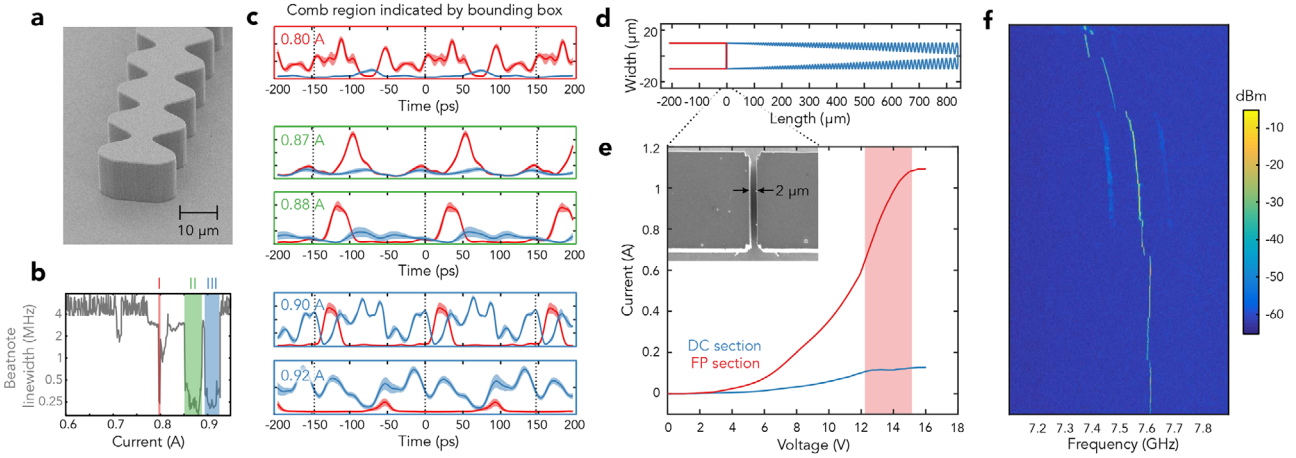

Figure 5. a) Scanning electron microscope image of an integrated dispersion compensation cavity.[18] From https://www.rle.mit.edu/thz/research/mems-based-arrays-of-millimeter-receivers/. b) Linewidth of the RF signal emitted from the QCL as a function of bias, measured with a spectrum analyzer. Shaded areas labeled as I, II, and III indicate the regions of stable comb formation. c) Bias dependence of time-dependent intensities of the homogeneous frequency comb of panels a) and b). Lower lobe frequencies are marked in red, while upper lobe frequencies in blue. (b,c) Adapted with permission.[68] Copyright 2015, The Optical Society. d) Schematic of the two-section device with the *dc*-biased section marked in blue. e) Current–voltage characteristics for each section. The shaded area indicates the dynamic range of lasing. Inset: SEM image of the device. f) Intermode beatnote map collected while biasing the *dc* section to the optimal point for each bias of the Fabry Perot cavity. (d–f) Adapted with permission.[70] Copyright 2017, The Optical Society.

signals have similar average powers, but the red lobe's power is concentrated in narrow time-domain pulses while the blue lases nearly continuously (Figure 5c).[68] This identifies an important peculiar aspect of THz FCs, that is, the existence of a regime of strong amplitude modulation than can coexist with frequency modulation.[18]

The relationship between FWM and group velocity dispersion (GVD) in the QCL cavity plays a key role in the stability of the QCL FC over the whole laser operation range. Gain medium engineering can indeed allow a flat top gain, though only at a specific bias point, meaning that the gain medium itself influences the dispersion dynamics at other biases.

Adapting the bias-dependent contribution to the chromatic dispersion is, hence, essential for achieving a stable frequency comb emission with relatively high-intensity modes over the full QCL bias range.

However, controlling the bias-dependent dispersion compensation in the far-infrared is a very challenging task. Current schemes include both passive and active architectures. Successful passive approaches include a dispersion compensator[18] integrated in the laser cavity that, through the chirping of the frequency and the tapering of the amplitude, allows reaching FC operation over 29% of the QCL operational regime. Alternative passive configurations include tunable Gires–Tournois interferometers (GTI), comprising a movable gold mirror coupled with the back QCL facet, which, as a result of a partial compensation of the total group delay dispersion (GDD), increases by 15% the bias range in which the QCL operates as a FC.[69]

Active approaches usually make use of external cavities, for example including a *dc*-biased section[70] (Figure 5d–e) capable to allow FC operation over the whole bias range (Figure 5f), at the price of a reduced optical bandwidth (≤ 400 GHz) and limited

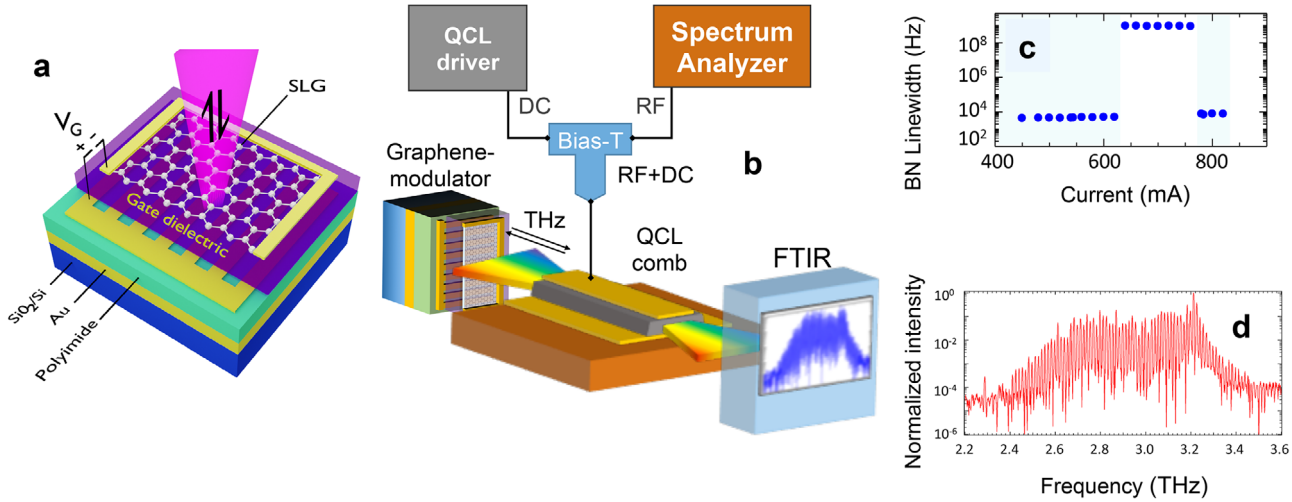

Figure 6. a) Schematic of the SLG modulator comprising a metal grating-SLG capacitor with pitch *p*, patterned on a polyimide layer with an underneath Au layer. b) Schematic experimental setup: an external cavity configuration is defined by coupling the SLG modulator with the THz QCL back facet at a 50 μm distance. The light back-reflected by the modulator is injected into the QCL cavity, while the radiation out-coupled from the front facet is sent into a Fourier-Transform InfraRed (FTIR) spectrometer. c) Intermode beatnote linewidths plotted as a function of QCL driving current when the QCL is coupled with a SLG modulators having a grating period $p = 10$ μm; d) FTIR emission spectrum measured at 15 K, under vacuum with ≈0.075cm^{-1} resolution, whilst driving the QCL in CW with 780 mA under the experimental configuration of panel (c). Adapted with permission.[72] Copyright 2021, Wiley-VCH.

(μW) optical power outputs[70] or, lithographically designed to define a Gires–Tournois interferometer,[71] which is effective in compensating the GDD only at a specific bias point.[71]

Extending THz QCL FC operation over the entire range of biases up to the operation point (J_{max}) corresponding to the maximum optical power output with a broad (>1 THz) spectral coverage is a very challenging task. Recently, complex architectures, exploiting unusual device technologies or making use of combined material systems, have been developed.

Grating-gated modulators employing single layer graphene (SLG) have been recently coupled with a THz QCL in an external cavity configuration with the purpose to act as passive dispersion compensators. A metallic grating coupler, patterned on a polyimide layer that acts as a quarter wave resonance cavity, is used as a gate electrode to tune SLG.[72] The polyimide thickness (14 μm) is chosen to match the $n\lambda/4$ waveguide mode with n (= 1) integer number (quarter wave mode) at the central frequency ν = 2.85 THz (wavelength λ = 105 μm) of the multimode QCL. The metal grating couples with the quarter wave mode and defines the modulator resonant frequency, while acting as the counter electrode of the SLG capacitor (**Figure 6**a). Once integrated with the THz QCLs (Figure 6b), the modulator induces a visible amplitude modulation in the THz QCL and leads to FC operation over 35% of the QCL operational range, as revealed by the intermode beatnote maps (Figure 6c), with 98 equidistant optical modes and with a spectral coverage of ≈1.2 THz (Figure 6d).

An alternative architecture relies on the integration, in an external cavity configuration, of a THz QCL with a tightly coupled, on-chip, solution-processed, 65nm thick graphene saturable-absorber reflector (**Figure 7**a), prepared by liquid phase exfoliation of graphite in a water/surfactant solution. The saturable absorber reflector provided to be effective in preserving the phase coherence between lasing modes, even in the regime in which FWM in unable to provide dispersion compensation.[73] The gapless nature of graphene, its *ps* recovery time,[74] limited saturation fluence,[75] and flexibility that makes it prone to fabrication[76] and integration,[77] are potential for nonlinear optical experiments. Specifically, graphene can be employed to introduce intensity dependent losses into a laser cavity, when tightly coupled to it, as a result of its fast saturable absorption nature.[78,79] It has been indeed proved that 80% transparency modulation can be reached, as a result of the intraband induced absorption bleaching.[78]

FWM in a THz QCL, can be generated by fast saturable gain, which induces a frequency modulated output, or loss, associated with amplitude modulation.[66] Both mechanisms are typically present,[68] in a THz QCL. Comb formation can therefore result from the saturable absorption effect occurring inside graphene,[73] but also from the fact that the graphene features Fresnel reflection on its surface. This latter component is spatially separated from the saturable absorption occurring in the SLG and can then contribute to frequency comb stabilization through the same mechanism as the fast saturable gain in the active region, leading to frequency modulation. The saturable absorption in graphene[78] helps regularizing the remaining amplitude modulation.

Figure 7d plots the free running electrical beatnote map acquired on the integrated system sketched in Figure 7a, measured with a bias-tee, and recorded with a radio frequency (RF) spectrum analyzer. A single and narrow (Figure 7b,c) intermode beatnote, signature of stable comb operation through 55% of the bias range of the QCL is visible. At the peak optical power, where a single and narrow beat note is retrieved, the QCL emits 8 mW of CW power with 90 equally spaced optical modes covering a 0.94 THz spectral bandwidth, and shows (Figure 7d) more than three-decades of reduction of phase-noise over an additional 15% of this range. Such a devices promise to be a key metrological

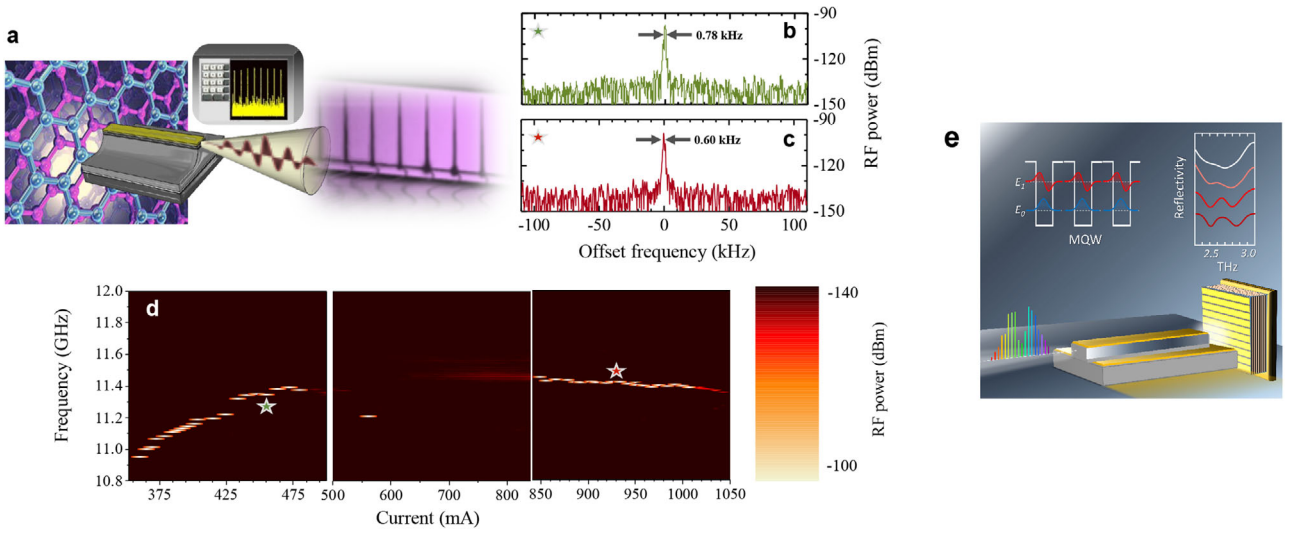

Figure 7. a) Schematic diagram of a THz QCL comprising an on-chip graphene saturable absorber (GSA) reflector. Intermode beatnote measured at b) $I = 456$ mA and c) at $I = 928$ mA. d) Intermode beatnote map measured in continuous wave and 15 K, as a function of QCL current. The beatnote signal is extracted from the bias line with a bias-tee and it is recorded with an RF spectrum analyzer (Rohde and Schwarz FSW; RBW: 500 Hz, video bandwidth (VBW): 500 Hz, sweep time (SWT): 20 ms, RMS acquisition mode). The two star symbols correspond to the driving currents of panels (b) and (c). Adapted with permission.[73] Copyright 2020, American Chemical Society. e) Visual representation of a FC THz QCL comprising an ultrafast THz polaritonic reflector, exploiting intersubband cavity polaritons, integrated with broad bandwidth (2.3–3.8 THz) heterogeneous THz QCL. Adapted with permission.[85] Copyright 2021, Wiley-VCH.

tool for dual-comb THz spectroscopy[80–83] and hyperspectral imaging,[84] paving the way to deliver an all-in-one miniaturized, high-power electrically pumped FC in the far-infrared.

An alternative elegant approach relies in an external cavity configuration comprising an ultrafast THz polaritonic reflector, exploiting intersubband (ISB) cavity polaritons, and a broad bandwidth (2.3–3.8 THz) heterogeneous THz QCL.[85] The polaritonic mirror comprises a semiconductor multi-quantum-well (MQW) heterostructure, embedded in a ≈2 μm size double metal cavity, having a top Au grating with 16 μm period, that fix the optical coupling to the MQW.[85] A radiation polarized orthogonal to the grating lines, impinging at normal incidence, induces a fringe electric field within the MQW heterostructure that satisfies the ISB transition selection rule.[86]

By pumping the polaritonic mirror with a THz laser, a visible spectral change of the intersubband reflectivity spectrum in the 2–3 THz spectral window[86] at intensities larger than 7.8 W cm^{-2} is observed, with a progressive bleaching of the upper polaritonic mode.[86] This effect can be used to modify the cavity dispersion of a QCL (Figure 7e). Once using the polaritonic mirror as the back mirror of an external cavity, comprising the free-running THz QCL FCs, the GDD can be tuned by exploiting the light-induced bleaching of the ISB-based THz polaritons. This causes the spectral reshaping of the QCL emission and drive the QCL in a stable FC regime over an operational range up to 38%. This can be unveiled in the intermode beatnote that appears single and narrow (down to 700 Hz).[85] The proposed concept has a high potential for the development of mode-locked THz micro-lasers exploiting saturable absorption in the tightly coupled external cavity. This promises broad application impacts in high-speed quantum communication and ultrafast science.

Although the presented characterization of the driving current-dependent intermodal beat-note (IBN), with single and sharp (linewidths in the kHz range) IBN, provides an initial assessment of the FC operation in a QCL, demanding applications in quantum science require information about the stability of the Fourier phases of the QCL FC modes. This can be targeted by more precise optical techniques as the shifted-wave interference Fourier-transform spectroscopy (SWIFT),[87,88] which relies on measuring the phase difference between adjacent FC modes (**Figure 8**a) in the phase domain or via the Fourier analysis of the comb emission (FACE).[89,80] In SWIFT, the phase relation of continuous portions of the FC spectrum is retrieved via the cumulative sum on the phases measured via FTIR spectroscopy. The inherent need for a mechanical scan does not allow for a simultaneous analysis of the phases but, provided that all the measurement frequency chain is properly calibrated, SWIFT unambiguously reveals the phase stability during a precise measurement window. The FACE technique, based on a multi-heterodyne detection scheme, allows real-time tracing of the phases of the modes emitted by the FC, thus working even if the comb presents spectral gaps (Figure 8b). While the variation of each phase retrieved with this experimental procedure is notably low,[80] this does not hold true for the deviation of the phases from the linear trend, that is expected for a conventional, pulse-emitting, FC. The measured sets of amplitudes and phases, when used to reconstruct the emitted field, give emission profiles that are amplitude and frequency modulated. Heterodyne techniques have been also applied to intracavity room temperature DFG QCL-FC, giving an insight on their coherence level.[90]

An accurate exploitation of THz QCL FC for quantum metrological applications requires a tight phase referencing to a well-suited frequency standard, of both the QCL-FC modes spacing

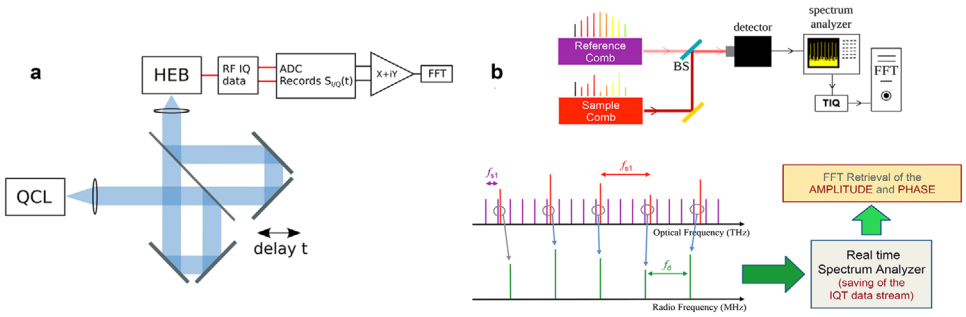

Figure 8. Schematics of the SWIFT (a) and FACE (b) optical techniques.

and frequency offset that, in turn, requires two distinctive orthogonal actuators to be stabilized. However, to date, the only available fast actuator, acting simultaneously on both parameters, is the QCL driving current. By exploiting the driving current actuator in two distinctive frequency ranges,[80] one can overcome such a constrain, reaching phase stabilization of the THz QCL-FC: in this latter case, the emission linewidth of each comb mode can reach values as low as ≈2 Hz in 1s, with the possibility to make each comb line individually frequency tunable. The possibility to employ visible light as further actuator on QCL-FCs degrees of freedom has been also recently investigated by the small optical frequency tuning (SOFT) technique.[91]

As a final note, a novel mechanism of FC generation in QCLs, suggested by studies performed in the mid-IR,[92] has been recently proposed and relies of the emission of optical modes separated by higher harmonics of the cavity free spectral range (FSR) (Figure 8a), rather than adjacent cavity modes as typical of fundamental comb regime (Figure 8b). Such a state, known as harmonic comb regime, can be reached by varying the QCL driving current so that it first reaches a state of high single-mode intracavity intensity and then, when its intensity is large enough, it is driven at an instability threshold caused by the $\chi^{(3)}$ population pulsation non-linearity, favoring the appearance of modes separated by tens of FSRs from the first lasing mode. Recently, such an approach has been successfully exploited to devise a self-starting harmonic frequency comb, with a THz repetition rate, in a QCL.[92] This is reached through temporal modulation of the population inversion that induces the parametric contribution to the gain.[93] Harmonic combs have interesting perspectives for exploring quantum correlation effects in the far-infrared.

5. Perspectives

Quantum cascade laser sources can open intriguing perspectives in quantum science with an impact on all main areas, from sensing and metrology to communication, computation and simulation. Regarding sensing and metrology, we have here discussed the main achievements in terms of quantum-limited frequency noise operation and phase/frequency absolute referencing. The next step is THz-QCLs operation below the classical limits and we have shown that several strategies can allow achieving this goal. We expect that a THz quantum photonic platform based on QCLs will enable generation of non-classical radiation and/or demonstration of entanglement among different comb-emitted modes, in close analogy with squeezing effects demonstrated more than 25 years ago in semiconductor bipolar laser diodes.[94] Already at that time, sub-shot noise operation of the laser current driver was the key and, nowadays, this is addressed even in commercially available devices (e.g., https://www.ppqsense.it/products/qubecl-laser-controllers/qubecl/low-noise).

Moreover, a powerful way to endow QCL-FCs of quantum properties is expected to be FWM that can ensure intrinsic quantum correlation effects in the laser cavity. Along this line, quantum simulation with atoms (fermions) of electron transport in the quantum cascade laser structure has been recently proposed, to optimize the QCL design.[30] Interaction of THz radiation with matter represents an additional, twofold, motivation for its exploitation in quantum technologies applications. Firstly, most molecular rotational transitions are resonant with THz radiation; secondly, THz propagation in free space undergoes orders of magnitude less scattering effects than visible light, due to the much longer wavelength: the drawback of THz propagation in air, however, is represented by the strong water vapor absorption.

Control of rotational degrees of freedom in simple molecules, by using THz coherent radiation, will represent the pathway for their full manipulation and exploitation, especially for quantum simulation, computation and metrology.[95–97]

The Shannon formula C (bit s^{-1}) = $W\log_2(1 + S/N)$ (where C is the data rate, or information capacity, W is the available bandwidth and S/N the signal-to-noise ratio) defines the achievable data rate in any communication system. It is known that data traffic is exponentially increasing, worldwide, especially due to the ever-increasing use of wireless devices [e.g., Cisco The Zettabyte Era: Trends and Analysis 1–24 (Cisco and/or its affiliates, 2014)]. Therefore, classical wireless communication networks are already moving, since several years, toward THz frequencies, to increase data rates to several hundred Gbit s^{-1} exploiting the higher carrier frequencies of the sub-mm spectral range, not yet allocated for telecom applications.[98,99] This trend is also motivated by several other advantages of THz frequency radiation as compared to even higher frequencies infrared carriers: the higher tolerance to misalignment and the much lower scattering losses in foggy/dusty/smoky conditions for free-space propagation beams.

Also quantum communication, exploiting quantum-key-distribution (QKD) to provide an intrinsic security endowed by quantum mechanics, is expected to follow a similar trend, for the future. Therefore, THz QCLs can play a major role also for such applications. Considering the strong absorption of water vapor of large parts of the THz spectrum, inter-satellite communication

in space can be an ideal environment for THz QCL deployment, as well as very short-range (<a few meters) outdoor applications. Carrier signals at low frequencies, generated by a THz QCL, can also be ideal to enable wireless implementations of quantum key distributions in a few-photon communications system, where the carrier photon need to display higher, or similar, energies, as compared to the thermal background noise. In addition, indoor and outdoor quantum key distribution applications can allow addressing the goal of beyond fifth-generation ultra-secure wireless communications systems.

Furthermore, THz quantum entanglement distributions are viable deployment options in the micro-satellite communication context, where no water-vapor absorption is present. Continuous-variable entangled states can become major strategic tools for several target outcomes. In particular, they can be potentially configured as the founding blocks for future implementation of quantum computation protocols, quantum teleportation or to increase capacity, robustness and security of selected free-space quantum communication channels.

The development of a fully integrated, QCL-based, quantum platform also requires engineering appropriate detectors, having a background noise significantly lower than the shot noise limit of the radiation coupled, a sufficiently wide dynamic range, important when QCL is operating in continuous-wave radiation, and a high-quantum efficiency. Although direct IR detection schemes have very recently started to be investigated,[100] performance limitations seem to be quite severe, yet, as compared to the best available silicon detectors in the near-IR. If emerging superconductive technologies could provide answers for the mid-IR range,[101,102] it is still unclear if they can be extended to the THz range. Moreover, the ultracold operation temperature of such class of detectors can represent a serious obstacle to their widespread adoption. An alternative technology could be represented by high-efficiency nonlinear up-conversion of THz radiation to the near IR region, where the best detectors are available. In this respect, it is noteworthy that, while a number of different down-conversion schemes set-ups have been demonstrated from the near IR to the THz, both continuous wave and pulsed,[103–106] THz-to-optical conversion has been mostly limited to specific applications, with low conversion efficiency, yet.[107] The main expected challenge for such an approach is represented by the use of high laser intensities for highly efficient conversion, requiring appropriate optics and nonlinear materials, with transparency/reflectivity adequate for generation and propagation of widely different wavelengths, in the near/far IR ranges.

Moreover, 2D materials combined with QCLs can also open appealing perspectives in quantum science. By stacking layered materials into a sandwich configuration, an incredibly broad range of optical properties can be reached once the material is embedded in a device. As an example, depending on the way they are stacked, the resulting heterostructure can work as a light reflector, transmitter or absorber. In addition, these materials are showing unique potential for their further integration into quantum photonic circuits as single photon emission and detection.

2D materials well integrate with QCLs, either coupled with their emission facet[73,108] or intracavity, both in conventional Fabry–Perot architectures and in more exotic random structures.[109]

In this context, QCLs offer an interesting playground for the development of functionalized, compact and coherent, solid state-based FIR sources, exploiting the giant optical nonlinearities of 2D materials, integrated on chip. This promises to open new domains in quantum science, such as quantum control of condensed matter as, for example, of the model atom-in-semiconductor system Si:P that has been proposed for quantum computing applications.[110] In this case, whilst the qubit is encoded in the nuclear splitting in the microwave range, the 1s-2p transition of the trapped *P* atom lies in the far-IR region, around 8THz. This transition has been used to coherently control the qubit state.

The scalable integration of quantum devices into integrated quantum networks has so far showed major limitations due to the incompatibility of materials, growth processes, miniaturization, and integration of various quantum components on existing mature Si or CMOS platforms, key ingredients in current quantum technologies. QCLs and 2D materials offer a unique perspective to build up integrated quantum platforms in the far-infrared and in the millimeter wave regime. It is indeed worth mentioning that compact, low noise mm-wave generation can be easily achieved using mode-locked THz frequency combs.[111]

Finally, near-field microscopy could also fundamentally benefit of powerful THz QCLs for fundamental investigations at the nanoscale, as inspecting charge carrier density,[112] plasmon–polariton[113,114] and phonon–polariton.[115,116] THz QCL based near-field microscopy can allow mapping the spatial variation and the bias dependence of local currents induced by light illumination, allowing to study the photocarrier transport or the electronic band bending, or to unveiling fundamental physical phenomena in semiconductors, superconductors or bi-dimensional (2D) materials as graphene, phosphorene or transition metal dichalcogenides, that can guide the design of quantum detectors and single photon sources exploiting such a novel class of 2D quantum materials. Combining high sample quality and advanced experimental techniques[117,118] can enable investigation of electron–electron interactions in graphene and stimulate novel strategies for quantum sensing of collective excitations in 2D materials,[119,120] using the QCL as a powerful quantum source, with an adequate thermal management.[121]

Acknowledgements

This work was supported by the European Research Council through the ERC Consolidator Grant (681379) SPRINT. The authors acknowledge L. Consolino for technical discussions.

Open Access Funding provided by Consiglio Nazionale delle Ricerche within the CRUI-CARE Agreement.

Conflict of Interest

The authors declare no conflict of interest.

Data Availability Statement

The data that support the findings of this study are available from the corresponding author upon reasonable request.

Keywords

metrology, quantum cascade lasers, quantum materials, quantum technologies, terahertz

Received: June 24, 2021
Revised: October 14, 2021
Published online: November 16, 2021

[1] J. L. O'Brien, A. Furusawa, J. Vučković, *Nat. Photonics* **2009**, *3*, 687.
[2] J. C. Loredo, C. Antón, B. Reznychenko, P. Hilaire, A. Harouri, C. Millet, H. Ollivier, N. Somaschi, L. De Santis, A. Lemaître, I. Sagnes, L. Lanco, A. Auffèves, O. Krebs, P. Senellart, *Nat. Photonics* **2019**, *13*, 803.
[3] L. Pezzè, A. Smerzi, M. K. Oberthaler, R. Schmied, P. Treutlein, *Rev. Mod. Phys.* **2018**, *90*, 035005.
[4] F. Arute, K. Arya, R. Babbush, D. Bacon, J. C. Bardin, R. Barends, R. Biswas, S. Boixo, F. G. S. L. Brandao, D. A. Buell, B. Burkett, Y. Chen, Z. Chen, B. Chiaro, R. Collins, W. Courtney, A. Dunsworth, E. Farhi, B. Foxen, A. Fowler, C. Gidney, M. Giustina, R. Graff, K. Guerin, S. Habegger, M. P. Harrigan, M. J. Hartmann, A. Ho, M. Hoffmann, T. Huang, et al., *Nature* **2019**, *574*, 505.
[5] N. W. Hendrickx, W. I. L. Lawrie, M. Russ, F. Van Riggelen, S. L. de Snoo, R. N. Schouten, A. Sammak, G. Scappucci, M. Veldhorst, *Nature* **2021**, *591*, 580.
[6] S. K. Liao, W.-Q. Cai, W.-Y. Liu, L. Zhang, Y. Li, J.-G. Ren, J. Yin, Q. Shen, Y. Cao, Z.-P. Li, F.-Z. Li, X.-W. Chen, L.-H. Sun, J.-J. Jia, J.-C. Wu, X.-J. Jiang, J.-F. Wang, Y.-M. Huang, Q. Wang, Y.-L. Zhou, L. Deng, T. Xi, L. Ma, T. Hu, Q. Zhang, Y.-A. Chen, N.-L. Liu, X.-B. Wang, Z.-C. Zhu, C.-Y. Lu, et al., *Nature* **2017**, *549*, 43.
[7] V. Giovannetti, S. Lloyd, L. Maccone, *Nat. Photonics* **2011**, *5*, 222.
[8] M. Kutas, B. Haase, P. Bickert, F. Riexinger, D. Molter, G. von Freymann, *Sci. Adv.* **2020**, *6*, eaaz8065.
[9] J. Wang, F. Sciarrino, A. Laing, M. G. Thompson, *Nat. Photonics* **2020**, *14*, 273.
[10] J. Faist, F. Capasso, D. Sivco, C. Sirtori, A. Hutchinson, A. Cho, *Science* **1994**, *264*, 553.
[11] M. S. Vitiello, G. Scalari, B. Williams, P. De Natale, *Opt. Express* **2015**, *23*, 5167.
[12] M. S. Vitiello, A. Tredicucci, *Adv. Phys. X* **2021**, *6*, 1893809.
[13] M. Rösch, G. Scalari, M. Beck, J. Faist, *J. Nat. Photonics* **2014**, *9*, 42.
[14] L. H. Li, K. Garrasi, I. Kundu, Y. J. Han, M. Salih, M. S. Vitiello, A. G. Davies, E. H. Linfield, *Electron. Lett.* **2018**, *54*, 1229.
[15] M. Brandstetter, C. Deutsch, M. Krall, H. Detz, D. C. Macfarland, T. Zederbauer, A. M. Andrews, W. Schrenk, G. Strasser, K. Unterrainer, *Appl. Phys. Lett.* **2013**, *103*, 171113.
[16] M. Wienold, B. Röben, L. Schrottke, R. Sharma, A. Tahraoui, K. Biermann, H. T. Grahn, *Opt. Express* **2014**, *22*, 3334.
[17] M. S. Vitiello, L. Consolino, S. Bartalini, A. Taschin, A. Tredicucci, M. Inguscio, P. De Natale, *Nat. Photonics* **2012**, *6*, 525.
[18] D. Burghoff, T.-Y. Y. Kao, N. Han, C. W. Chan, X. Cai, Y. Yang, D. J. Hayton, J. R. Gao, J. L. Reno, Q. Hu, *Nat. Photonics* **2014**, *8*, 462.
[19] A. Forrer, M. Franckié, D. Stark, T. Olariu, M. Beck, J. Faist, G. Scalari, *ACS Photonics* **2020**, *7*, 784.
[20] A. Di Gaspare, L. Viti, H. E. Beere, D. A. Ritchie, M. S. Vitiello, *Nanophotonics* **2021**, *10*, 181.
[21] K. Garrasi, F. P. Mezzapesa, L. Salemi, L. Li, L. Consolino, S. Bartalini, P. De Natale, A. G. Davies, E. H. Linfield, M. S. Vitiello, *ACS Photonics* **2019**, *6*, 73.
[22] M. Rösch, M. Beck, M. J. Süess, D. Bachmann, K. Unterrainer, J. Faist, G. Scalari, *Nanophotonics* **2018**, *7*, 237.
[23] Q. Lu, D. Wu, S. Sengupta, S. Slivken, M. Razeghi, *Sci. Rep.* **2016**, *6*, 23595.
[24] S. Jung, A. Jiang, Y. Jiang, K. Vijayraghavan, X. Wang, M. Troccoli, M. A. Belkin, *Nat. Commun.* **2014**, *5*, 4267.
[25] Y. Jiang, K. Vijayraghavan, S. Jung, F. Demmerle, G. Boehm, M. C. Amann, M. A. Belkin, *J. Opt.* **2014**, *16*, 094002.
[26] S. Jung, Y. Jiang, K. Vijayraghavan, A. Jiang, F. Demmerle, G. Boehm, X. Wang, M. Troccoli, M. C. Amann, M. A. Belkin, *IEEE J. Sel. Top. Quantum Electron.* **2015**, *21*, 134.
[27] K. Fujita, S. Jung, Y. Jiang, J. H. Kim, A. Nakanishi, A. Ito, M. Hitaka, T. Edamura, M. A. Belkin, *Nanophotonics* **2018**, *7*, 1795.
[28] S. Bartalini, L. Consolino, P. Cancio, P. De Natale, P. Bartolini, A. Taschin, M. De Pas, H. Beere, D. Ritchie, M. S. Vitiello, R. Torre, *Phys. Rev. X* **2014**, 021006.
[29] L. Consolino, F. Cappelli, M. Siciliani de Cumis, P. De Natale, *Nanophotonics* **2019**, *8*, 181.
[30] A. Trombettoni, F. Scazza, F. Minardi, G. Roati, F. Cappelli, L. Consolino, A. Smerzi, P. De Natale, *Adv. Quantum Technol.* **2021**, *4*, 2100044.
[31] M. Yamanishi, T. Edamura, K. Fujita, N. Akikusa, H. Kan, *IEEE J. Quantum Electron.* **2008**, *44*, 12.
[32] C. Henry, in *Coherence, Amplification, and Quantum Effects in Semiconductor Lasers* (Ed: Y. Yamamoto), Wiley, New York **1991**, p. 5.
[33] R. P. Green, J. H. Xu, L. Mahler, A. Tredicucci, F. Beltram, G. Giuliani, H. E. Beere, D. A. Ritchie, *Appl. Phys. Lett.* **2008**, *92*, 071106.
[34] D. S. Elliott, R. Roy, S. J. Smith, *Phys. Rev. A* **1982**, *26*, 12.
[35] A. Campa, L. Consolino, M. Ravaro, D. Mazzotti, M. S. Vitiello, S. Bartalini, P. De Natale, *Opt. Express* **2015**, *23*, 3751.
[36] S. Bartalini, S. Borri, P. Cancio, A. Castrillo, I. Galli, G. Giusfredi, D. Mazzotti, L. Gianfrani, P. De Natale, *Phys. Rev. Lett.* **2010**, *104*, 083904.
[37] H. W. Hübers, S. G. Pavlov, H. Richter, A. D. Semenov, L. Mahler, A. Tredicucci, H. E. Beere, D. A. Ritchie, *Appl. Phys. Lett.* **2006**, *89*, 061115.
[38] H. M. Wiseman, *Phys. Rev. A – At. Mol. Opt. Phys.* **1999**, *60*, 4083.
[39] L. A. Dunbar, R. Houdrá, G. Scalari, L. Sirigu, M. Giovannini, J. Faist, *Appl. Phys. Lett.* **2007**, *90*, 141114.
[40] C. Walther, G. Scalari, M. Beck, J. Faist, *Opt. Lett.* **2011**, *36*, 2623.
[41] S. Barbieri, P. Gellie, G. Santarelli, L. Ding, W. Maineult, C. Sirtori, R. Colombelli, H. E. Beere, D. A. Ritchie, *Nat. Photonics* **2010**, *4*, 636.
[42] D. Weidmann, L. Joly, V. Parpillon, D. Courtois, Y. Bonetti, T. Aellen, M. Beck, J. Faist, D. Hofstetter, *Opt. Lett.* **2003**, *28*, 704.
[43] L. Consolino, S. Jung, A. Campa, M. De Regis, S. Pal, J. H. Kim, K. Fujita, A. Ito, M. Hitaka, S. Bartalini, P. De Natale, M. A. Belkin, M. S. Vitiello, *Sci. Adv.* **2017**, *3*, e1603317.
[44] L. Consolino, A. Taschin, P. Bartolini, S. Bartalini, P. Cancio, A. Tredicucci, H. E. Beere, D. A. Ritchie, R. Torre, M. S. Vitiello, P. De Natale, *Nat. Commun.* **2012**, *3*, 1040.
[45] M. Ravaro, S. Barbieri, G. Santarelli, V. Jagtap, C. Manquest, C. Sirtori, S. P. Khanna, E. H. Linfield, *Opt. Express.* **2012**, *20*, 25654.
[46] A. Barkan, F. K. Tittel, D. Mittleman, R. Dengler, P. H. Siegel, G. Scalari, L. Ajili, J. Faist, H. E. Beere, E. H. Linfield, A. G. Davies, D. A. Ritchie, *Opt. Lett.* **2004**, *29*, 575.
[47] S. Barbieri, J. Alton, H. E. Beere, E. H. Linfield, D. A. Ritchie, S. Withington, G. Scalari, L. Ajili, J. Faist, *Opt. Lett.* **2004**, *29*, 1632.
[48] U. U. Graf, C. E. Honingh, K. Jacobs, J. Stutzki, *J. Infrared Milli. Terahertz Waves* **2015**, *36*, 896.
[49] M. Tonouchi, *Nat. Photonics* **2007**, *1*, 97.
[50] L. D. Carr, D. DeMille, R. V. Krems, J. Ye, *New J. Phys.* **2009**, *11*, 055049.
[51] A. L. Betz, R. T. Boreiko, B. S. Williams, S. Kumar, Q. Hu, J. L. Reno, *Opt. Lett.* **2005**, *30*, 1837.
[52] H. Richter, S. G. Pavlov, A. D. Semenov, L. Mahler, A. Tredicucci, H. E. Beere, D. A. Ritchie, D. A. H. W. Hübers, *Appl. Phys. Lett.* **2005**, *96*, 071112.
[53] Y. Ren, J. N. Hovenier, M. Cui, D. J. Hayton, J. R. Gao, T. M. Klapwijk, S. C. Shi, T. Y. Kao, Q. Hu, J. L. Reno, *Appl. Phys. Lett.* **2012**, *100*, 041111.

[54] H. W. Hübers, R. Eichholz, S. G. Pavlov, H. Richter, *J. Infrared Milli. Terahertz Waves* **2015**, *34*, 325.
[55] L. H. Enloe, J. L. Rodda, *Proc. IEEE* **1965**, *53*, 165.
[56] D. Rabanus, U. U. Graf, M. C. Phillips, O. Ricken, J. Stutzki, B. Vowinkel, M. C. Wiedner, C. Walther, M. Fischer, J. Faist, *Opt. Express* **2009**, *17*, 1159.
[57] P. Khosropanah, A. Baryshev, W. Zhang, W. Jellema, J. N. Hovenier, J. R. Gao, T. M. Klapwijk, D. G. Paveliev, B. S. Williams, S. Kumar, Q. Hu, J. L. Reno, B. Klein, J. L. Hesler, *Opt. Lett.* **2009**, *34*, 2958.
[58] M. Ravaro, C. Manquest, C. Sirtori, S. Barbieri, G. Santarelli, K. Blary, J.-F. Lampin, S. P. Khanna, E. H. Linfield, *Opt. Lett.* **2011**, *36*, 3969.
[59] S. Barbieri, P. Gellie, G. Santarelli, L. Ding, W. Maineult, C. Sirtori, R. Colombelli, H. Beere, D. A. Ritchie, *Nat. Photonics* **2010**, *4*, 636.
[60] T. Udem, R. Holzwarth, T. W. Hänsch, *Nature* **2002**, *416*, 233.
[61] T. Yasui, S. Yokoyama, H. Inaba, K. Minoshima, T. Nagatsuma, T. Araki, *IEEE J. Sel. Top. Quantum Electron.* **2011**, *17*, 191.
[62] M. S. Vitiello, A. Tredicucci, *Adv. Phys. X* **2021**, *6*, 1893809.
[63] R. Holzwarth, T. Udem, T. W. Hänsch, J. C. Knight, W. J. Wadsworth, P. S. J. Russell, *Phys. Rev. Lett.* **2000**, *85*, 2264.
[64] D. J. Jones, S. A. Diddams, J. K. Ranka, R. S. Windeler, A. J. Stentz, J. L. Hall, S. T. Cundiff, *Science* **2000**, *288*, 635.
[65] J. Faist, G. Villares, G. Scalari, M. Rösch, C. Bonzon, A. Hugi, M. Beck, *Nanophotonics* **2016**, *5*, 272.
[66] J. B. Khurgin, Y. Dikmelik, A. Hugi, J. Faist, *Appl. Phys. Lett.* **2014**, *104*, 081118.
[67] M. S. Vitiello, L. Consolino, M. Inguscio, P. De Natale, *Nanophotonics* **2021**, *10*, 187.
[68] D. Burghoff, Y. Yang, D. J. Hayton, J. R. Gao, J. L. Reno, Q. Hu, *Opt. Express* **2015**, *23*, 1190.
[69] F. P. Mezzapesa, V. Pistore, K. Garrasi, L. Li, G. A. Davies, E. H. Linfield, S. S. Dhillon, M. S. Vitiello, *Opt. Express* **2019**, *27*, 20231.
[70] Y. Yang, D. Burghoff, J. Reno, Q. Hu, *Opt. Lett.* **2017**, *42*, 3888.
[71] F. Wang, H. Nong, T. Fobbe, V. Pistore, S. Houver, S. Markmann, N. Jukam, M. I. Amanti, C. Sirtori, S. Moumdji, R. Colombelli, L. Li, E. H. Linfield, G. A. Davies, J. Mangeney, J. Tignon, S. S. Dhillon, *Laser Photonics Rev.* **2017**, *11*, 1700013.
[72] A. Di Gaspare, E. A. A. Pogna, L. Salemi, O. Balci, A. R. Cadore, S. Maruti Shinde, L. Li, C. Di Franco, A. Giles Davies, E. H. Linfield, A. C. Ferrari, G. Scamarcio, M. S. Vitiello, *Adv. Funct. Mater.* **2020**, 2008039.
[73] F. P. Mezzapesa, K. Garrasi, J. Schmidt, L. Salemi, V. Pistore, L. Li, A. G. Davies, E. H. Linfield, M. Riesch, C. Jirauschek, T. Carey, F. Torrisi, A. C. Ferrari, M. S. Vitiello, *ACS Photonics* **2020**, *7*, 3489.
[74] D. Brida, A. Tomadin, C. Manzoni, Y. J. Kim, A. Lombardo, S. Milana, R. R. Nair, K. S. Novoselov, A. C. Ferrari, G. Cerullo, M. Polini, *Nat. Commun.* **2013**, *4*, 1987.
[75] Z. Sun, T. Hasan, F. Torrisi, D. Popa, G. Privitera, F. Wang, F. Bonaccorso, D. M. Basko, A. C. Ferrari, *ACS Nano* **2010**, *4*, 803.
[76] F. Bonaccorso, A. Lombardo, T. Hasan, Z. Sun, L. Colombo, A. C. Ferrari, *Mater. Today* **2012**, *15*, 564.
[77] A. Tredicucci, M. S. Vitiello, *IEEE J. Sel. Top. Quantum Electron.* **2014**, *20*, 130.
[78] V. Bianchi, T. Carey, L. Viti, L. Li, E. H. Linfield, A. G. Davies, A. Tredicucci, D. Yoon, P. G. Karagiannidis, L. Lombardi, F. Tomarchio, A. C. Ferrari, F. Torrisi, M. S. Vitiello, *Nat. Commun.* **2017**, *8*, 15763.
[79] H. A. Hafez, S. Kovalev, K. J. Tielrooij, M. Bonn, M. Gensh, D. Turchinovich, *Adv. Opt. Mater.* **2020**, *8*, 1900771.
[80] L. Consolino, M. Nafa, M. De Regis, F. Cappelli, K. Garrasi, F. P. Mezzapesa, L. Li, A. G. Davies, E. H. Linfield, M. S. Vitiello, S. Bartalini, P. De Natale, *Commun. Phys.* **2020**, *3*, 69.
[81] Z. Li, W. Wan, K. Zhou, X. Liao, S. Yang, Z. Fu, J. C. Cao, H. Li, *Phys. Rev. Appl.* **2021**, *12*, 044068.
[82] H. Li, Z. Li, W. Wan, K. Zhou, X. Liao, S. Yang, C. Wang, J. C. Cao, H. Zeng, *ACS Photonics* **2020**, *7*, 49.
[83] Y. Zhao, Z. Li, K. Zhou, X. Liao, W. Guan, W. Wan, S. Yang, J. C. Cao, D. Xu, S. Barbieri, H. Li, *Laser Photonics Rev.* **2021**, *15*, 2000498.
[84] L. A. Sterczewski, J. Westberg, Y. Yang, D. Burghoff, J. Reno, Q. Hu, G. Wysocki, *Optica* **2019**, *6*, 766.
[85] F. P. Mezzapesa, L. Viti, L. Li, V. Pistore, S. S. Dhillon, A. G. Davies, E. H. Linfield, M. S. Vitiello, *Laser Photon. Rev.* **2021**, 2000575.
[86] J. Raab, F. P. Mezzapesa, L. Viti, N. Dessmann, L. K. Diebel, L. Li, A. G. Davies, E. H. Linfield, C. Lange, R. Huber, M. S. Vitiello, *Nat. Commun.* **2020**, *11*, 1.
[87] D. Burghoff, Y. Yang, D. J. Hayton, J. R. Gao, J. L. Reno, Q. Hu, *Opt. Express* **2015**, *23*, 1190.
[88] Z. Han, J. Ren, D. Burghoff, *Opt. Express* **2020**, *28*, 6002.
[89] F. Cappelli, L. Consolino, G. Campo, J. Galli, D. Mazzotti, A. Campa, M. Siciliani de Cumis, P. Cancio Pastor, R. Eramo, M. Rösch, M. Beck, G. Scalari, J. Faist, P. De Natale, S. Bartalini, *Nat. Photonics* **2019**, *13*, 562.
[90] Q. Lu, F. Wang, D. Wu, S. Slivken, M. Razeghi, *Nat. Commun.* **2019**, *10*, 2403.
[91] L. Consolino, A. Campa, M. De Regis, F. Cappelli, G. Scalari, J. Faist, M. Beck, M. Rösch, S. Bartalini, P. De Natale, *Lasers Photon. Rev.* **2021**, *15*, 2000417.
[92] D. Kazakov, M. Piccardo, Y. Wang, P. Chevalier, T. S. Mansuripur, F. Xie, C. Zah, K. Lascola, A. Belyanin, F. Capasso, *Nat. Photonics* **2017**, *11*, 789.
[93] T. S. Mansuripur, C. Vernet, P. Chevalier, G. Aoust, B. Schwarz, F. Xie, C. Caneau, K. Lascola, C.-en. Zah, D. P. Caffey, T. Day, L. J. Missaggia, M. K. Connors, C. A. Wang, A. Belyanin, F. Capasso, *Phys. Rev. A* **2016**, *94*, 063807.
[94] F. Marin, A. Bramati, E. Giacobino, T.-C. Zhang, J.-Ph. Poizat, J.-F. Roch, P. Grangier, *Phys. Rev. Lett.* **1995**, *75*, 4606.
[95] J. A. Blackmore, L. Caldwell, P. D. Gregory, E. M. Bridge, R. Sawant, J. Aldegunde, J. Mur-Petit, D. Jaksch, J. M. Hutson, B. E. Sauer, M. R. Tarbutt, S. L. Cornish, *Quantum Sci. Technol.* **2019**, *4*, 014010.
[96] L. Anderegg, L. W. Cheuk, Y. Bao, S. Burchesky, W. Ketterle, K.-K. Ni, J. M. Doyle, *Science* **2019**, *365*, 1156.
[97] S. S. Kondov, C.-H. Lee, K. H. Leung, C. Liedl, I. Majewska, R. Moszynski, T. Zelevinsky, *Nat. Phys.* **2019**, *15*, 1118.
[98] T. Nagatsuma, G. Ducournau, C. C. Renaud, *Nat. Photon.* **2016**, *10*, 371.
[99] T. Kürner, S. Priebe, *J. Infrared Millim. Terahertz Waves* **2014**, *35*, 53.
[100] T. Gabbrielli, F. Cappelli, N. Bruno, N. Corrias, S. Borri, P. De Natale, A. Zavatta, *Opt. Express* **2021**, *29*, 14536.
[101] V. B. Verma, B. Korzh, A. B. Walter, A. E. Lita, R. M. Briggs, M. Colangelo, Y. Zhai, E. E. Wollman, A. D. Beyer, J. P. Allmaras, H. Vora, D. Zhu, E. Schmidt, A. G. Kozorezov, K. K. Berggren, R. P. Mirin, S. W. Nam, M. D. Shaw, *APL Photonics* **2021**, *6*, 056101.
[102] L. You, *Nanophotonics* **2020**, *9*, 2673.
[103] J. Neu, C. A. Schmuttenmaer, *J. Appl. Phys.* **2018**, *124*, 231101.
[104] D. Mazzotti, P. Cancio, G. Giusfredi, P. De Natale, M. Prevedelli, M. Bellini, G. Gagliardi, *Opt. Lett.* **2005**, *30*, 997.
[105] M. De Regis, S. Bartalini, M. Ravaro, D. Calonico, P. De Natale, L. Consolino, *Phys. Rev. Appl.* **2018**, *10*, 064041.
[106] F. W. Wise, A. Chong, W. H. Renninger, *Laser Photon. Rev.* **2008**, *2*, 11.
[107] S. Ummethala, T. Harter, K. Koehnle, Z. Li, S. Muehlbrandt, Y. Kutuvantavida, J. Kemal, P. Marin-Palomo, J. Schaefer, A. Tessmann, S. K. Garlapati, A. Bacher, L. Hahn, M. Walther, T. Zwick, S. Randel, W. Freude, C. Koos, *Nat. Photonics* **2019**, *13*, 519.
[108] H. Li, M. Yan, W. Wan, T. Zhou, K. Zhou, Z. Li, J. Cao, Q. Yu, K. Zhang, M. Li, J. Nan, B. He, H. Zeng, *Adv. Sci.* **2019**, *6*, 1900460.
[109] S. Biasco, H. E. Beere, D. A. Ritchie, L. Li, A. G. Davies, E. H. Linfield, M. S. Vitiello, *Light: Sci. Appl.* **2019**, *8*, 43.

[110] P. T. Greenland, S. A. Lynch, A. F. G. van der Meer, B. N. Murdin, C. R. Pidgeon, B. Redlich, N. Q. Vinh, G. Aeppli, *Nature* **2010**, *465*, 1057.
[111] V. Pistore, H. Nong, P.-B. Vigneron, K. Garrasi, S. Houver, L. Li, A. G. Davies, E. H. Linfield, J. Tignon, J. Mangeney, R. Colombelli, M. S. Vitiello, S. S. Dhillon, *Nat. Commun.* **2021**, *12*, 1427.
[112] E. A. A. Pogna, M. Asgari, V. Zannier, L. Sorba, L. Viti, M. S. Vitiello, *Light: Sci. Appl.* **2020**, *9*, 189.
[113] J. Chen, M. Badioli, P. Alonso-González, S. Thongrattanasiri, F. Huth, J. Osmond, M. Spasenović, A. Centeno, A. Pesquera, P. Godignon, A. Z. Elorza, N. Camara, F. J. García de Abajo, R. Hillenbrand, F. H. L. Koppens, *Nature* **2012**, *487*, 77.
[114] Z. Fei, A. S. Rodin, G. O. Andreev, W. Bao, A. S. Mcleod, M. Wagner, L. M. Zhang, Z. Zhao, M. Thiemens, G. Dominguez, M. M. Fogler, A. H. C. Neto, C. N. Lau, F. Keilmann, D. N. Basov, *Nature* **2012**, *486*, 82.
[115] P. Li, M. Lewin, A. V. Kretinin, J. D. Caldwell, K. S. Novoselov, T. Taniguchi, K. Watanabe, F. Gaussmann, T. Taubner, *Nat. Commun.* **2015**, *6*, 7507.
[116] T. Low, A. Chaves, J. D. Caldwell, A. Kumar, N. X. Fang, P. Avouris, T. F. Heinz, F. Guinea, L. Martin-Moreno, F. Koppens, *Nat. Mater.* **2017**, *16*, 182.
[117] M. C. Giordano, S. Mastel, C. Liewald, L. L. Columbo, M. Brambilla, L. Viti, A. Politano, K. Zhang, L. Li, A. G. Davies, E. H. Linfield, R. Hillenbrand, F. Keilmann, G. Scamarcio, M. S. Vitiello, *Opt. Express* **2018**, *26*, 18423.
[118] U. Siciliani De Cumis, J. H. Xu, L. Masini, R. Degl'Innocenti, P. Pingue, F. Beltram, A. Tredicucci, M. S. Vitiello, P. A. Benedetti, H. E. Beere, D. A. Ritchie, *Opt. Express* **2012**, *20*, 21924.
[119] E. A. A. Pogna, L. Viti, A. Politano, M. Brambilla, G. Scamarcio, M. S. Vitiello, *Nature Commun.* **2021**, https://doi.org/10.1038/s41467-021-26831-6.
[120] L. Viti, A. Politano, M. S. Vitiello, *APL Materials* **2017**, *5*, 035602.
[121] M. S. Vitiello, G. Scamarcio, V. Spagnolo, J. Alton, S. Barbieri, C. Worrall, H. E. Beere, D. A. Ritchie, C. Sirtori, *Appl. Phys. Lett.* **2016**, *89*, 021111.

Miriam Serena Vitiello, group leader of the Terahertz photonics and optoelectronics group at NEST – Nanoscience Institute of the National Research Council (CNR), is director of research at CNR and adjunct professor of condensed matter physics at Scuola Normale Superiore (IT). She is member of the Scientific Council of INRIM, of the CNR DSFTM, and of the CEITEC center (Czech Republic). She is the recipient of prestigious awards (Friedel-Volterra Medal 2020), Sapio Research-and-Innovation Award (2018), Guido Dorso Award (2016), SPIE Early Career Award (2015), "Sergio Panizza" award of the Italian Physical Society (2012)). She is co-author of more than 250-refereed papers on international journals, holds 1 patent and delivered more than 100 invited/plenary talks at international conferences.

Paolo De Natale is research director at the National Institute of Optics – INO (Italian National Research Council – CNR) and member of LENS, Firenze, Italy. In 2007–2021, he was director of INO-CNR (former INOA). He is the Italian representative in the Quantum Community Network (QCN) Board of the EU Flagship on Quantum Technologies. He is author of more than 360 publications, owns 9 patents, and is a co-founder of two former CNR spin-off companies, ppqSense srl and QTI srl. He is fellow of IEEE (since 2011) and OSA (since 2015).